Title
Validation of on- and off-axis neutral beam current drive against experiment in DIII-D[a]

Journal
Physics of Plasmas, 16(9)

ISSN
1070-664X

Authors
Park, JM
Murakami, M
Petty, CC
et al.

Publication Date
2009-10-12

DOI
10.1063/1.3213614

Validation of on- and off-axis neutral beam current drive against experiment in DIII-D[a)]

J. M. Park,[1,b)] M. Murakami,[1] C. C. Petty,[2] W. W. Heidbrink,[3] T. H. Osborne,[2] C. T. Holcomb,[4] M. A. Van Zeeland,[2] R. Prater,[2] T. C. Luce,[2] M. R. Wade,[2] M. E. Austin,[5] N. H. Brooks,[2] R. V. Budny,[6] C. D. Challis,[7] J. C. DeBoo,[2] J. S. deGrassie,[2] J. R. Ferron,[2] P. Gohil,[2] J. Hobirk,[8] E. M. Hollmann,[9] R. M. Hong,[2] A. W. Hyatt,[2] J. Lohr,[2] M. J. Lanctot,[10] M. A. Makowski,[4] D. C. McCune,[5] P. A. Politzer,[2] H. E. St John,[2] T. Suzuki,[11] W. P. West,[2] E. A. Unterberg,[12] and J. H. Yu[9]

[1]*Oak Ridge National Laboratory, P.O. Box 2008, Oak Ridge, Tennessee 37831, USA*
[2]*General Atomics, P.O. Box 85608, San Diego, California 92186-5608, USA*
[3]*Department of Physics and Astronomy, University of California, Irvine, California 92697-4575, USA*
[4]*Lawrence Livermore National Laboratory, Livermore, California 94551, USA*
[5]*Fusion Research Center, University of Texas at Austin, Austin, Texas 78712 USA*
[6]*Princeton Plasma Physics Laboratory, Princeton, New Jersey 05843, USA*
[7]*Euratom/UKAEA Fusion Association, Culham Science Centre, Abingdon, Oxon OX14 3DB, United Kingdom*
[8]*Max-Planck-Institut fur Plasmaphysik, IPP-EURATOM Association, 85748 Garching, Germany*
[9]*University of California at San Diego, La Jolla, California 92093, USA*
[10]*Columbia University, New York, New York 10027, USA*
[11]*Japan Atomic Energy Agency, 801-1, Mukouyama, Naka, Ibaraki-ken 311-0193, Japan*
[12]*Oak Ridge Institute for Science Education, Oak Ridge, Tennessee 37831-0117, USA*

(Received 27 May 2009; accepted 10 August 2009; published online 28 September 2009)

Neutral beam current drive (NBCD) experiments in DIII-D using vertically shifted plasmas to move the current drive away from the axis have clearly demonstrated robust off-axis NBCD. Time-dependent measurements of magnetic field pitch angles by the motional Stark effect diagnostic are used to obtain the evolution of the poloidal magnetic flux, which indicates a broad off-axis NBCD profile with a peak at about half the plasma minor radius. In most cases, the measured off-axis NBCD profile is consistent with calculations using an orbit-following Monte Carlo code for the beam ion slowing down including finite-orbit effects provided there is no large-scale magnetohydrodynamic activity such as Alfvén eigenmodes modes or sawteeth. An alternative analysis method shows good agreement between the measured pitch angles and those from simulations using transport-equilibrium codes. Two-dimensional image of Doppler-shifted fast ion D_α light emitted by neutralized energetic ions shows clear evidence for a hollow profile of beam ion density, consistent with classical beam ion slowing down. The magnitude of off-axis NBCD is sensitive to the alignment of the beam injection relative to the helical pitch of the magnetic field lines. If the signs of toroidal magnetic field and plasma current yield the proper helicity, both measurement and calculation indicate that the efficiency is as good as on-axis NBCD because the increased fraction of trapped electrons reduces the electron shielding of the injected ion current, in contrast with electron current drive schemes where the trapping of electrons degrades the efficiency. The measured off-axis NBCD increases approximately linearly with the injection power, although a modest amount of fast ion diffusion is needed to explain an observed difference in the NBCD profile between the measurement and the calculation at high injection power. © *2009 American Institute of Physics*. [doi:10.1063/1.3213614]

I. INTRODUCTION

Neutral beam injection (NBI) is a robust method for heating and current drive (CD) in tokamak plasmas since it does not depend on any resonance conditions or coupling conditions at the plasma edge. Neutral beam CD (NBCD) is a dominant noninductive CD from external sources in DIII-D, as well as in many other tokamaks.[1]

Off-axis CD plays a crucial role in advanced tokamak (AT) scenarios.[2,3] For steady-state operation, all of the plasma current must be driven noninductively (without a transformer). The leading approach to the steady-state scenario utilizes the naturally hollow profile generated by the bootstrap current.[4] Since the bootstrap current profile may not perfectly match the optimal current profile for high fusion performance, a flexible, localized, and efficient source of noninductive current is needed for control. Experimentally, such high-performance discharges have been demonstrated in DIII-D; however, the duration is usually limited by the evolution of the current profile to an unstable state.[5,6] Experimental measurements and simulations of these dis-

[a)]Based on an invited talk given at the APS DPP Meeting in Dallas, November 2008. Paper VI2 2, Bull. Am. Phys. Soc. **53**, 317 (2008).
[b)]Invited speaker.

charges have indicated that these discharges could be extended to near steady state if the current profile were maintained by replacing the remaining Ohmic current (30%–40% of the total current) near the half radius with externally driven current.[7] The needed off-axis current can be supplied by electron cyclotron CD or by NBCD. If NBI could provide substantial off-axis CD by off-axis injection, the parameter space available for AT scenario development would be greatly increased.[8]

Recently, off-axis NBCD has been reported in several tokamaks such as ASDEX-U,[9,10] JT-60U,[11,12] MAST,[13,14] and JET.[15] ASDEX-U reported a lack of localization in off-axis NBCD due to anomalous fast ion transport. Simulations of the expected change in the magnetic field pitch angles during off-axis NBI did not agree with measurements above 5 MW of injection power. JT-60U observed a spatially localized off-axis NBCD profile with 2 MW NBI power. The total amount of the measured beam driven current was consistent with the theoretical calculation but a discrepancy in the CD location was found between the calculation and measurement. MAST reported noninductive current generation and control by off-axis NBCD with 3–3.5 MW NBI power in vertically displaced single-null divertor plasmas. The experimentally observed neutron rate and stored energy was significantly lower than the theoretical calculation, which was explained by anomalous fast ion diffusion correlated with $n=1$ fishbone activity. JET experiments have shown that the inversion radius and sawtooth size can be controlled by off-axis NBI.[15] Off-axis NBCD is planned for ITER,[16] so detailed comparison of theoretical models with experimental measurements is needed for accurate projection.

This paper describes experiments on DIII-D evaluating on- and off-axis NBCD using vertically shifted small plasmas. These experiments have utilized DIII-D's co- and counterinjection capability and recent diagnostic upgrades to study NB physics in great detail. In these studies, coinjection cases were compared to balanced-injection cases, with the noninductive current profile determined from the poloidal flux evolution measured by motional Stark effect (MSE) polarimetry.[17] The measured on- and off-axis NBCD profiles are then compared with the theoretical model using the orbit-following Monte Carlo code NUBEAM.[18] Particular attention has been paid to elucidating the differences in NBCD physics between on- and off-axis NBCD to help optimize off-axis NBCD as well as to demonstrate robust off-axis NBCD over a wide range of NBI power, owing to its importance in AT scenarios.

In Sec. II, experimental results are presented that demonstrate off-axis NBCD in DIII-D using vertically shifted plasmas to move the CD away from the axis. Experimental measurements from the MSE polarimetry, fast-ion D_α (FIDA) diagnostics, and neutron detector are compared with the theoretical calculations to validate the NBCD model in both on- and off-axis CD. In Sec. III, we discuss the importance of magnetic field direction in off-axis CD due to alignment of NB injection with the local magnetic field line. It is shown that the magnetic alignment affects the guiding center orbit of the beam ions and the NBCD efficiency. In Sec. IV, we discuss a detailed NB power scan to show the effects of anomalous fast ion transport on off-axis NBCD. Section V summarizes the main conclusions.

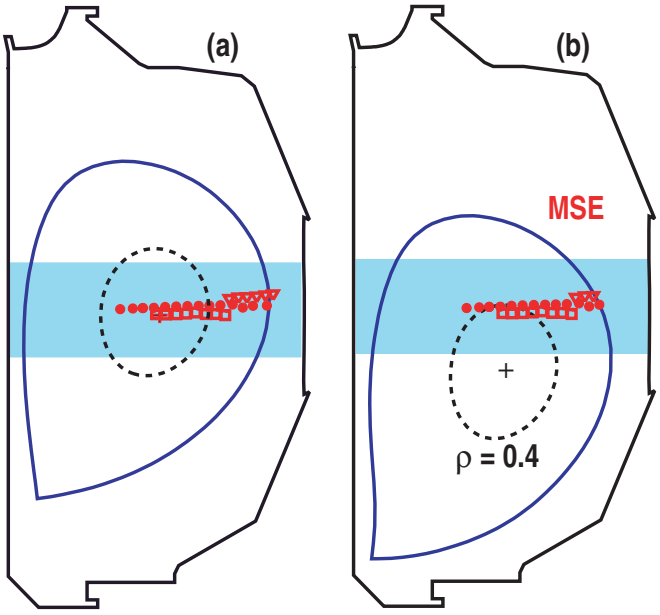

FIG. 1. (Color online) Plasma shape for (a) on- and (b) off-axis NBCD. The plasma center is shifted vertically downward to move NBCD off-axis. The locations of MSE measurement and the vertical extent of NB (shaded band) are shown.

II. DEMONSTRATION OF OFF-AXIS NBCD IN DIII-D

These NBCD experiments are done on DIII-D, typical parameters for which are major radius $R=1.7$ m, minor radius $a=0.55$ m, toroidal magnetic field strength $B_T=-2.1$ T, and plasma current $I_p=+0.9$ MA. Here, the sign conventions for B_T and I_p are that the positive direction is counterclockwise looking down from above. *H*-mode plasmas are used with a single null diverted plasma shape. Figure 1 shows the plasma shape developed particularly for these NBCD experiments. The plasma is shifted vertically downward by ~30 cm to move NBCD off-axis, since DIII-D NBs (Ref. 19) are injected horizontally through the midplane vessel ports. Then, beam ions are deposited mostly at $\rho \approx 0.5$, where ρ is the normalized minor radius proportional to the square root of the toroidal flux. The beams inject 81 keV deuterium atoms at a tangency radius of 1.15 m primarily to the cocurrent (+) direction using up to three beam sources. Each source injects ~2.5 MW. Short countercurrent beam pulses are added with an average power of ~0.5 MW for the MSE diagnostic, which utilizes both the co- and counter-injected NBs for improved current profile reconstruction. This codominated injection is compared to a fiducial balanced injection to cancel out systematic sources of error in CD analysis.

The most critical diagnostic for measuring the NBCD radial profile is MSE polarimetry using deuterium atoms injected by NBs, from which the magnetic field pitch angles at various major radii can be determined.[17] Even though the MSE channels cover only the outer radius region when the plasma is vertically shifted, the innermost location of MSE

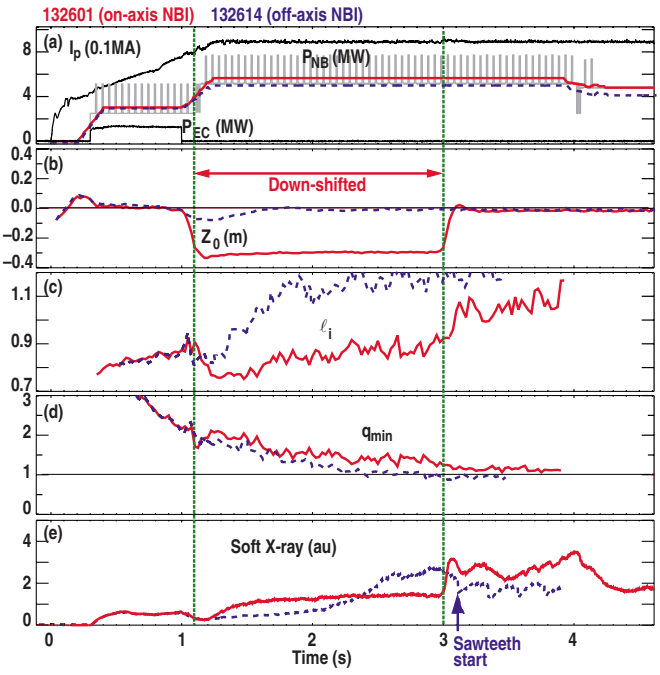

FIG. 2. (Color online) Typical time trace of ELMing H-mode discharge with on- (dashed line) and off-axis (solid line) NBCD: (a) plasma current, NB injection and ECH power, (b) vertical location of plasma center, (c) internal inductance ℓ_i, (d) safety factor $q_{\min}$, and (e) soft x-ray signal.

measurement ($\rho \approx 0.35$) is well inside the expected peak position of beam driven current. A number of diagnostics are used to determine the plasma profiles required for CD analysis; multipulse Thomson scattering for electron density (n_e) and temperature (T_e),[20] electron cyclotron emission (ECE) for T_e,[21] and charge exchange (CX) recombination emission from the carbon impurity for ion temperature (T_i), toroidal rotation (Ω), and effective ion charge (Z_{eff}).[22]

The time evolution of the main plasma parameters for a typical discharge is illustrated in Fig. 2. The discharge starts up with the L-mode (inside-wall limiter shape) midplane plasma. The plasma is shifted vertically downward, and maintained off-axis sufficiently long for CD measurements, then jogged back to the midplane quickly (within 50 ms) to measure the central plasma profiles inside $\rho \approx 0.4$. An L-H transition typically occurs just after the first vertical shift of plasma. Electron cyclotron heating (ECH) as well as NBI during the current plasma ramp up raises T_e and slows the resistive evolution of the current profile, delaying the onset of sawteeth. The global behavior of the discharge is consistent with the existence of off-axis CD that increases with co-NB power. Compared with a similar discharge in which the plasma center is kept at the midplane position throughout the discharge, NBI while the plasma is shifted generates off-axis NBCD that broadens the current profile, reducing the internal inductance ℓ_i significantly and keeping the safety factor $q_{\min}$ above unity. Sawteeth are absent in soft x-ray and ECE data during the off-axis NBI, and they reappear well after shifting to on-axis NBI. Systematic scans of NBI power have shown that the internal inductance decreases while $q_{\min}$ increases as the off-axis NB power increases, as expected.

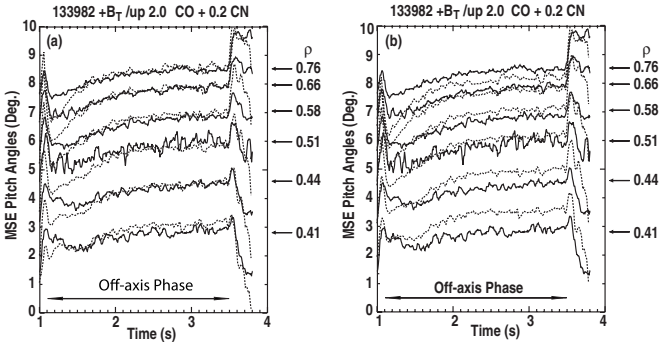

FIG. 3. Comparison of measured (solid curves) and simulated (dashed curves) evolution of the magnetic field pitch angles: (a) including off-axis NBCD and (b) excluding off-axis NBCD in TRANSP MSE simulation.

A. Local NBCD measurements

In Fig. 3(a), the time evolution of magnetic pitch angles from the MSE polarimetry are compared at different radii with the signals calculated by the coupled transport-equilibrium simulation of the poloidal flux evolution. The MSE simulation is performed by the TRANSP code[23] using the measured plasma profiles as input. The beam driven current is calculated by the orbit-following Monte Carlo code, NUBEAM without anomalous transport effects. The NCLASS model is employed for calculation of bootstrap current and the neoclassical conductivity.[24] Systematic offset errors of the calibration in the individual MSE channels are reduced by adjusting them to agree with calculated pitch angles, including the radial electric field (E_r) effects based on the force balance calculation, at an early time in another shot. Good agreement is found between the measured pitch angles and those from simulations. If the expected (off-axis) NBCD is not included, the simulations deviate significantly from the measured signals, as shown in Fig. 3(b).

The local NBCD profile is obtained quantitatively from the time evolution of poloidal magnetic flux.[25] The total parallel current $J_{\text{Tot}}(\rho)$ is determined from kinetic EFIT equilibrium reconstruction using the magnetic pitch angles from the MSE polarimetry and the external magnetic signals,[26] where the current profile in the edge pedestal is used as a constraint that is deduced from a time-dependent simulation of poloidal flux evolution using the ONETWO transport code.[27] The internal loop voltage profile is obtained from a time series of equilibrium reconstructions by taking the time derivative of the poloidal flux, $\partial\psi/\partial t$, which provides the Ohmic current profile $J_{\text{OH}}(\rho) = \sigma_{\text{Neo}} \partial\psi/\partial t$, where σ_{Neo} is the neoclassical conductivity from Ref. 28. The beam driven current is given by $J_{\text{NB}}(\rho) = J_{\text{Tot}}(\rho) - J_{\text{OH}}(\rho) - J_{\text{BS}}(\rho)$, where the bootstrap current $J_{\text{BS}}(\rho)$ is calculated by Sauter model.[29] The measured $J_{\text{NB}}(\rho)$ in Fig. 4 shows a broad profile with the peak at about half radius ($\rho \sim 0.55$). The error bars in Fig. 4 represent the random error from a time averaging procedure in the CD analysis. The random error is very small in this case due to the relatively long time interval (typically 800 ms) for averaging. However some systematic errors may come from uncertainty in Z_{eff} and in the theoretical models for bootstrap current and neoclassical conductivity.

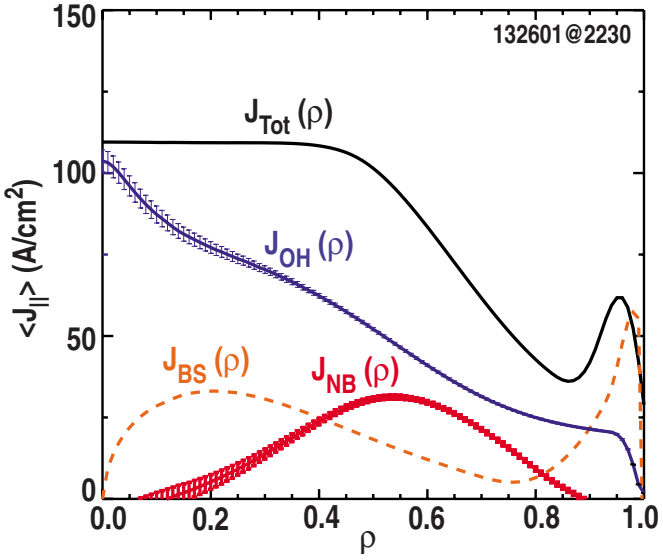

FIG. 4. (Color online) Radial profiles of total (J_{Tot}), Ohmic (J_{OH}), bootstrap (J_{BS}), and NB (J_{NB}) current for downward shifted plasma.

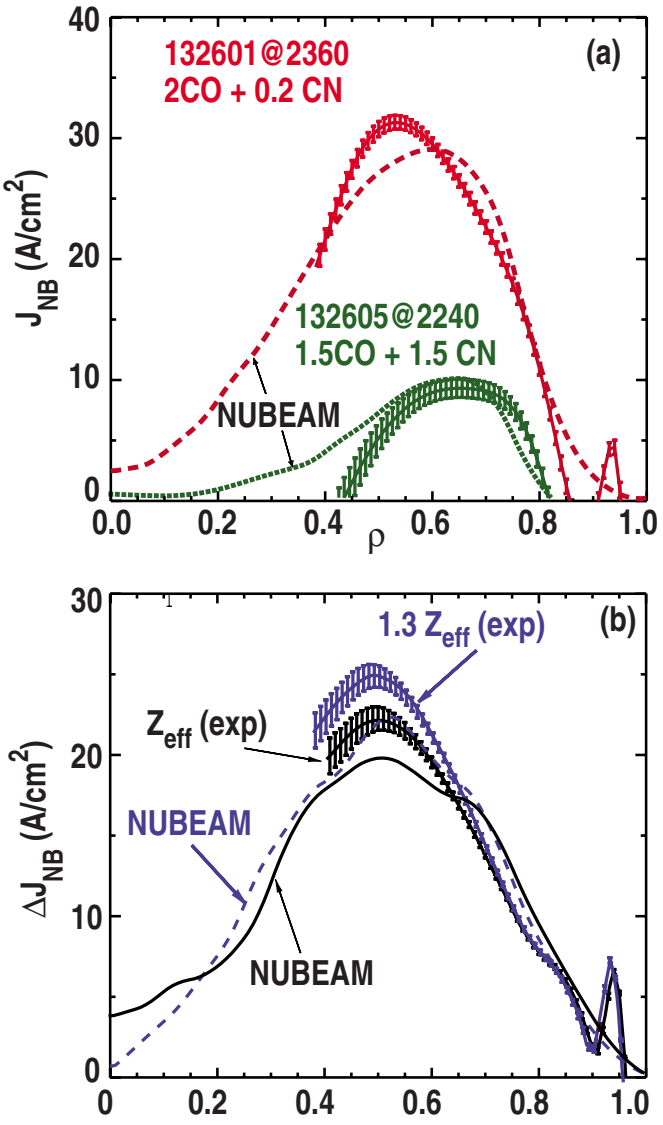

FIG. 5. (Color online) (a) NBCD analysis for co- and balanced NBI discharges, and (b) difference in NBCD profiles for co- and balanced injection. The curves with error bars are measurement and the curves without error bars are NUBEAM modeling.

Systematic uncertainties in the NBCD analysis, including the sensitivity to the choice of EFIT basis set, can be substantially reduced by subtracting a fiducial case.[30] This differential analysis compares two discharges with co- and balanced NBI at similar electron density (n_e) and temperature (T_e). Figure 5(a) shows the beam driven current profiles for two such discharges. Here, higher beam power is injected for the balanced NBI (1.5 co+1.5 counter) than the co-NBI (2 co+0.2 counter) in order to maintain similar n_e and T_e profiles (and similar β), since the confinement for balanced NBI is lower than that for co-NBI due to the lower $E\times B$ flow shear.[31] The measured NBCD profiles are in good agreement with the NUBEAM calculations for both co- and balanced NBI. It should be noted that a substantial amount of residual beam driven current (in the codirection for $\rho<0.8$ while in the counterdirection for $\rho>0.8$) was measured for the balanced NBI as expected, since the fast ion orbits of the counterbeam are shifted outward compared to those of the cobeam. As shown in Fig. 5(b), the difference in the measured beam-driven currents is not sensitive to the systematic errors. Even if we assume a systematic 30% error in the Z_{eff} profile, the difference in the current density between the co- and balanced injection does not change significantly and shows excellent agreement with the NUBEAM calculation. The differential analysis also significantly reduces the sensitivity to the bootstrap current model.

Figure 6 shows the beam-driven current profiles from the measurement and from NUBEAM calculations for the on- and off-axis beam injection cases. The on-axis NBCD profile is measured using a similar *H*-mode discharge in which the plasma center is kept at the midplane position throughout the discharge. Figure 7(a) compares the integrated beam driven current I_{NB} and the CD efficiency $\eta=[(\bar{n}_e I_{NB} R)/(P_{CO}-P_{CN})]$, where $\bar{n}_e$ is the line average density, R is the major radius, and P_{CO} and P_{CN} are injected NB powers for co- and counterinjection, respectively. The measured NBCD profile and integrated current agree well with the NUBEAM calculations for both on- and off-axis injection. Off-axis NBCD does not lose CD efficiency by going to a larger minor radius, which is an important aspect of NBCD primarily resulting from the trapped electron effect. Electron trapping, which increases with minor radius, reduces the collisionally driven electron current that tends to cancel the ion current. Therefore, electron shielding of off-axis NBCD is much lower than that for on-axis NBCD, as shown in Fig. 7(b). Trapping of electrons helps off-axis NBCD, unlike off-axis electron cyclotron (EC) CD scheme, where trapping reduces the CD efficiency.[32]

B. Fast ion density measurements

Dedicated shots for neutron and FIDA diagnostics[33,34] were made to study fast ion transport in off-axis NBI. Beam-blip techniques were used to measure prompt and delayed loss of fast ions.[35] Figure 8 shows the time behavior of the

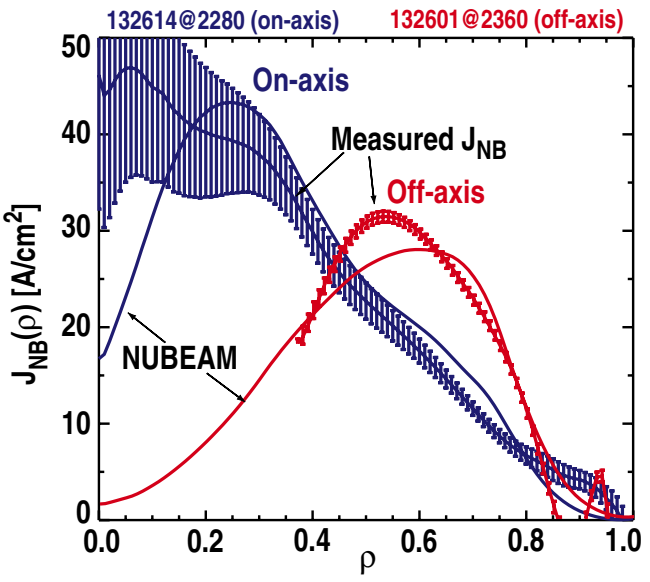

FIG. 6. (Color online) Comparison of measured NBCD profiles between on- (midplane plasma) and off-axis (downward shifted plasma) injection. The curves with error bars are measurement and the curves without error bars are NUBEAM modeling.

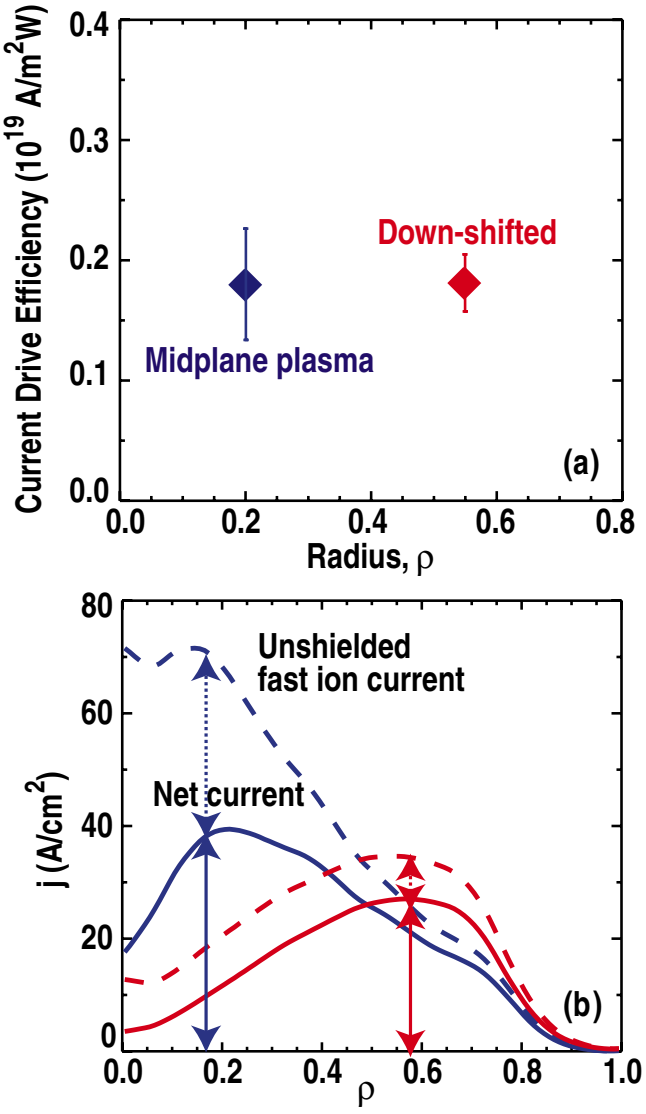

FIG. 7. (Color online) (a) Comparison of measured NBCD efficiency between on- (midplane plasma) and off-axis (downward shifted plasma) injection, (b) profiles of calculated unshielded fast ion current (dashed line), and net NBCD profiles (solid line) for on- and off-axis injection.

neutron rate for a 10 ms beam pulse during the off-axis injection phase. The neutron emission rises almost linearly during the beam pulse, then decays approximately exponentially after the pulse. The rise depends on the number of confined beam ions injected and the decay depends on the thermalization time for beam ions. The neutron data show that the beam ions are confined as expected for the off-axis injection. Figure 9 plots the experimental decay time for the on- and off-axis injection compared with the theoretical decay time calculated by the TRANSP/NUBEAM code. Both on- and off-axis decay times are consistent with the theory; the shorter decay time for off-axis deposition is due to the lower electron temperature.

The FIDA diagnostics use the Doppler-shifted D_α light from CX neutrals.[33,34] Multiple vertical viewing spectrometers measure the emission spectra at various radii that provide a radial profile of beam ion density and energy distribution.[33] The FIDA camera uses a narrowband interference filter on images at the plasma cross section that provides a two-dimensional (2D) spatial structure of the FIDA emission.[34] Beam modulation patterns are optimized for each FIDA diagnostic (see Ref. 34 for details). Figure 10 compares the 2D spatial structure of the FIDA emission for on- and off-axis injection, showing excellent agreement with the simulated signals, which are obtained by a FIDA modeling code[33] that calculates the theoretical number of photons observed by each pixel based on the calculated radial profile of beam ion density and energy distribution from the TRANSP/NUBEAM code. The FIDA images show a clear difference between the on- and off-axis injections, which are consistent with classical beam ion slowing down.

III. EFFECTS OF MAGNETIC FIELD ALIGNMENT ON OFF-AXIS NBCD

Alignment of the direction of beam injection with the local magnetic field helicity is important to the physics of NBCD. Recent theoretical work indicates that the off-axis NBCD is sensitive to the direction of toroidal magnetic field B_T, since it changes the alignment markedly in off-axis NBI configurations.[36] Figure 11 plots the velocity pitch angle of beam ions ($\lambda = v_\parallel/|\mathbf{v}|$) at their ionization location along the centerline of beamlets, where $v_\parallel$ is the projection of the beam ion velocity $\mathbf{v}$ onto the magnetic field line. If the direction of B_T is reversed, the pitch angle for the off-axis injection is altered significantly, while there is no appreciable change for the on-axis injection. Due to the radial component of the local poloidal magnetic field (B_R) at the birth location of beam ions for the off-axis injection, reversing the B_T direction makes a significant difference in the alignment as illustrated in Fig. 12(a). Note that the alignment of on-axis injec-

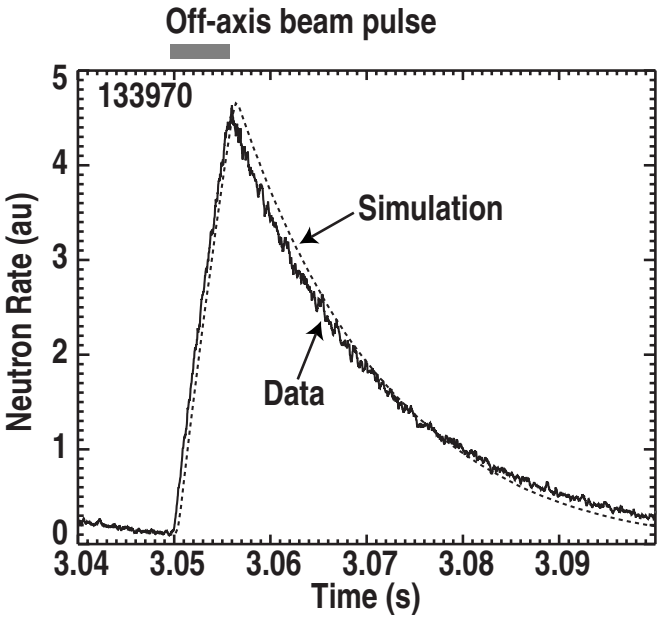

FIG. 8. Time trace of neutron rate for short beam pulse of off-axis injection (solid line: measurement and dotted line: NUBEAM modeling).

tion is related only to the toroidal field, since the poloidal magnetic field is small in the central region where the most beam ions are deposited. Even in the outer radius region of beam deposition for the on-axis injection, the vertical component (B_z) of poloidal field, which does not contribute to the alignment, is dominant over B_R [Fig. 12(b)]. Accordingly, a favorable B_T direction must exist for off-axis NBCD.

The magnetic field alignment effect was tested by reversing the sign of B_T for the downshifted plasma, or equivalently by shifting the plasma upward or downward with the same B_T direction. Figure 13 compares the measured NBCD profiles among the $-B_T$/downshifted (favorable alignment), $+B_T$/downshifted (unfavorable), and $+B_T$/upshifted (favorable) configurations. The injected beam power is 5.6 MW

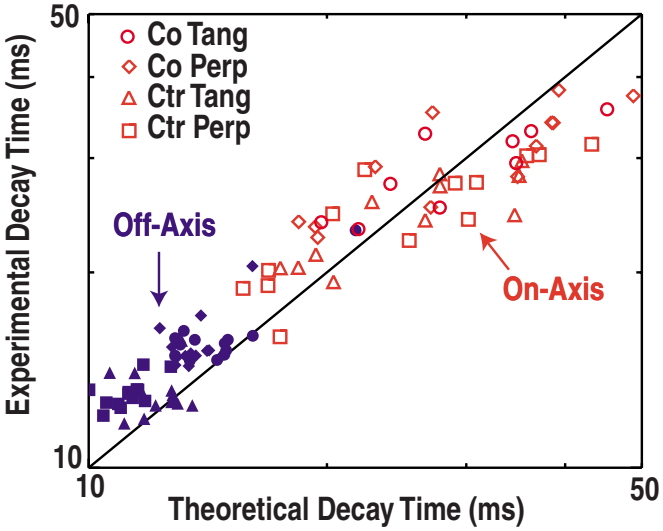

FIG. 9. (Color online) Comparison of experimental decay time of neutron rate with NUBEAM modeling for short beam pulses of on- (unfilled) and off-axis (filled) injection.

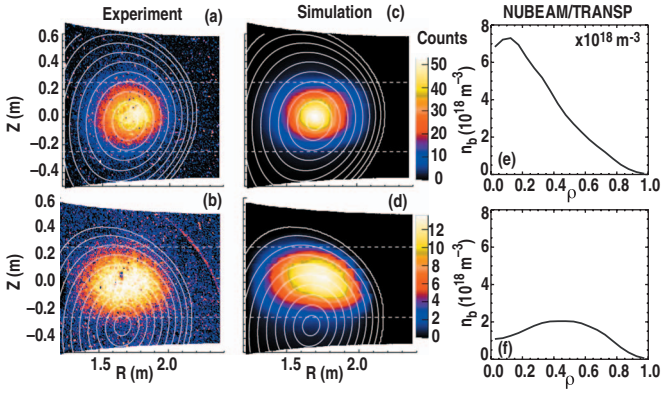

FIG. 10. (Color) Comparison of 2D FIDA images between (a) on- and (b) off-axis injection. Simulated FIDA signals [(c) on- and (d) off-axis injection] and radial profiles of beam ion density [(e) on- and (f) off-axis injection] obtained by NUBEAM modeling are shown.

for all cases. The NBCD profile in the unfavorable alignment configuration has a broader NBCD profile with a significantly reduced beam driven current. The measured difference in the NBCD profile is in good agreement with the theoretical prediction. The ratio of integrated current I_{NB} (unfavorable)/I_{NB} (favorable) is about 60%–65% in both measurement and theory.

Figure 14 displays the guiding center orbits of beam ions born at the same radial location $\rho=0.7$ but in the opposite B_T direction for the downshifted plasma. The beam ion in the $-B_T$ direction stays in a passing orbit during its slowing down, resulting in a well-localized CD. The guiding center orbit of beam ion in $+B_T$ direction; however, is a fat banana orbit with a wide width of $\Delta\rho_b \approx 0.3$ due to the mirror trapping in the toroidal geometry. The calculated difference in

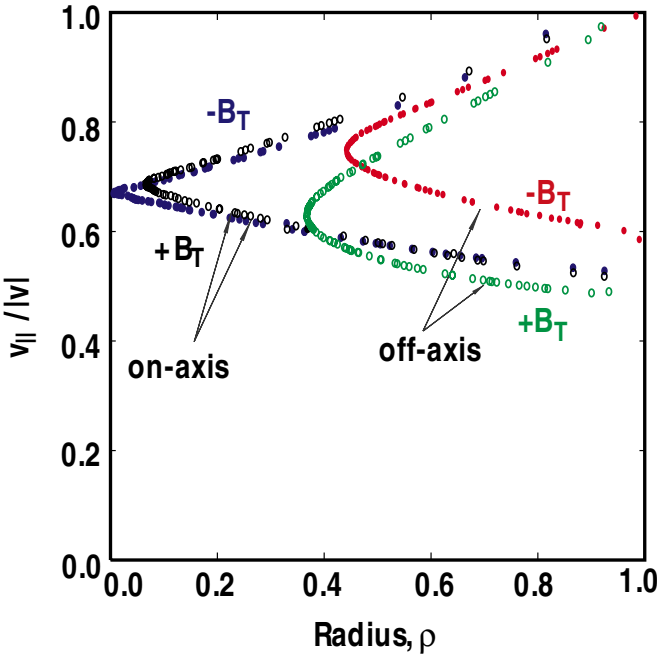

FIG. 11. (Color online) Velocity pitch angle of beam ions at their ionization location. The pitch angle for the off-axis injection is changed significantly if the direction of B_T is reversed.

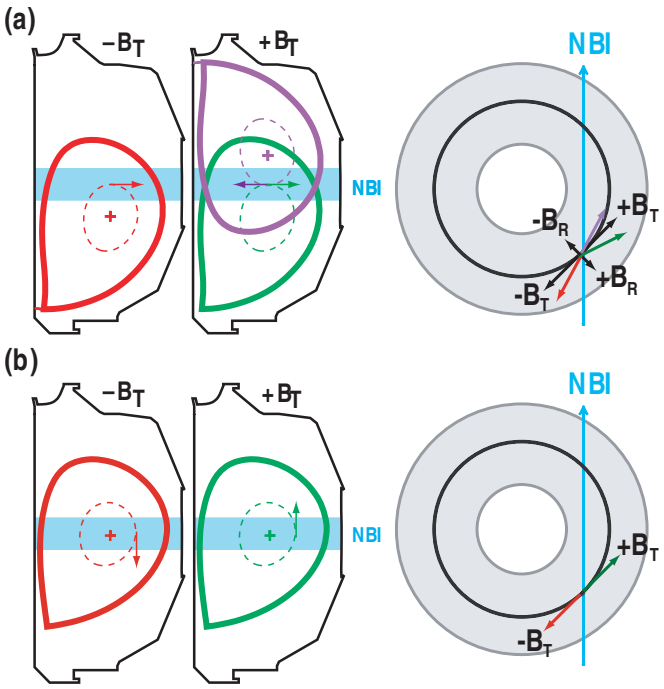

FIG. 12. (Color) Alignment of beam injection with local magnetic field helicity. (a) For off-axis injection, the magnetic configuration is well aligned (red, purple) or poorly aligned (green), depending on the sign of B_T and the vertical direction of shift. (b) For off-axis injection, the alignment does not depend on the sign of B_T.

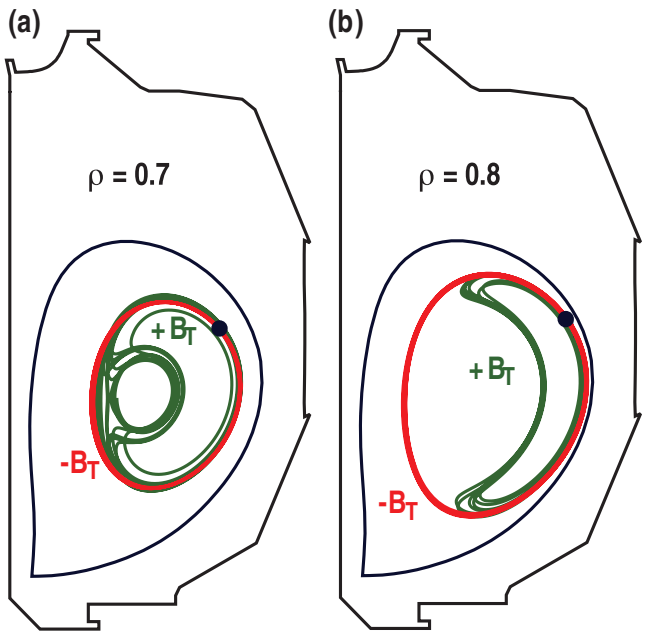

FIG. 14. (Color) Guiding center orbits of beam ions born at the same radial location [(a) ρ=0.7 and (b) ρ=0.8] but in the opposite B_T direction (green: $+B_T$, red: $-B_T$).

the trapping fraction of fast ions between $-B_T$ and $+B_T$ is ~10% at ρ=0.5 (Fig. 15). This magnetic trapping affects the off-axis NBCD in two ways: First, a beam ion traveling in the direction opposite to the plasma current during part of its trapped orbit tends to cancel the fast ion current. The fast ion distribution function for $+B_T$ reveals a higher population in the countercurrent direction (pitch angle <0). Second, the fat banana orbits place the beam ions near the axis where the electron shielding is higher, as shown in the calculated radial profile of beam ion density (Fig. 16). This difference between $+B_T$ and $-B_T$ was observed in FIDA measurements and inferred from neutron signals.[37] It should be noted that good off-axis NBCD does not necessarily mean good fast ion confinement or shifting the guiding center orbit inward.

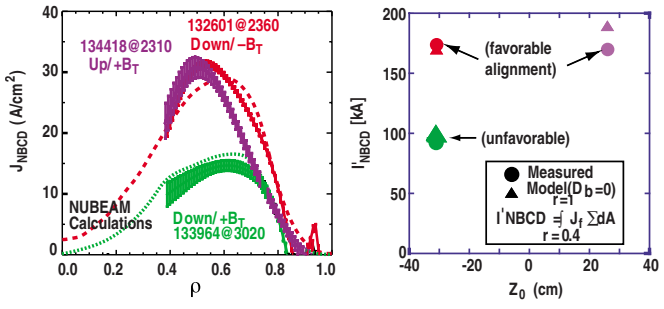

FIG. 13. (Color online) Measured NBCD profiles for $-B_T$/downshifted (favorable alignment), $+B_T$/downshifted (unfavorable), and $+B_T$/upshifted (favorable) configurations.

IV. EFFECTS OF ANOMALOUS FAST ION TRANSPORT ON OFF-AXIS NBCD

Anomalous fast ion transport tends to degrade the efficiency of off-axis NBCD and its localization. It was shown in Secs. II and III that the measured off-axis NBCD profiles are in excellent agreement with the classical beam ion slowing down model at the injection power P_{NB}=5.6 MW. This section describes a detailed NB power scan compared with the theoretical model to investigate effects of anomalous fast ion transport on off-axis NBCD. The theoretical calculation employs an *ad hoc* diffusion model with a spatially uniform coefficient D_b.

The measured integrated off-axis NBCD increases approximately linearly with the injection power in both favorable and unfavorable magnetic alignment configurations, as

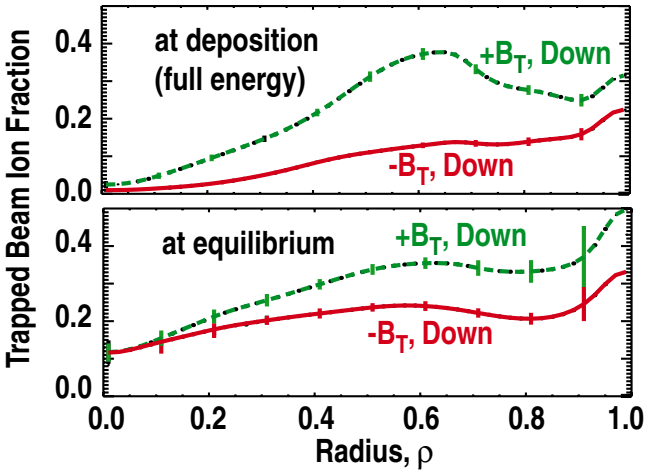

FIG. 15. (Color online) Comparison of fast ion trapping fraction (a) at deposition and (b) at equilibrium for $+B_T$ (dashed line) and $-B_T$ (solid line).

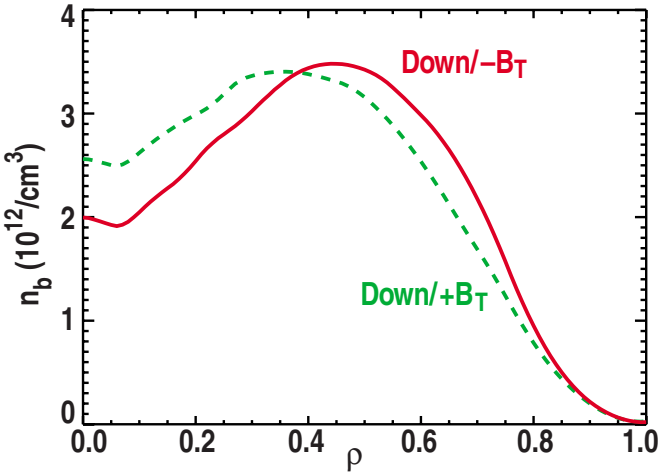

FIG. 16. (Color online) Radial profile of beam ion density for $+B_T$ (dashed line) and $-B_T$ (solid line).

shown in Fig. 17. For the highest injected power case, however, the measured NBCD deviates from the theoretical calculation with $D_b=0$ (Fig. 18). The integrated beam-driven current I_{NB} is smaller than the calculated value by ~20% at $P_{NB}=7.2$ MW. Detailed comparisons of these measurements with the theoretical calculation suggests that a modest amount of anomalous fast ion transport at high injection power can explain the reduction of I_{NB} relative to the classical prediction. Figure 19 compares the measured NBCD profile with the theoretical calculations with assumed D_b up to 0.5 m^2/s. Fast ion diffusion places particles near the axis, resulting in more diffused and inward shifted NBCD profile. The measured NBCD profile fits best with the theoretical calculation with $D_b=0$ and 0.3 m^2/s at $P_{NB}=5.6$ MW and 7.2 MW, respectively.

The radial profile of radiance from the vertical FIDA spectrometers as well as the neutron rate deviate from the

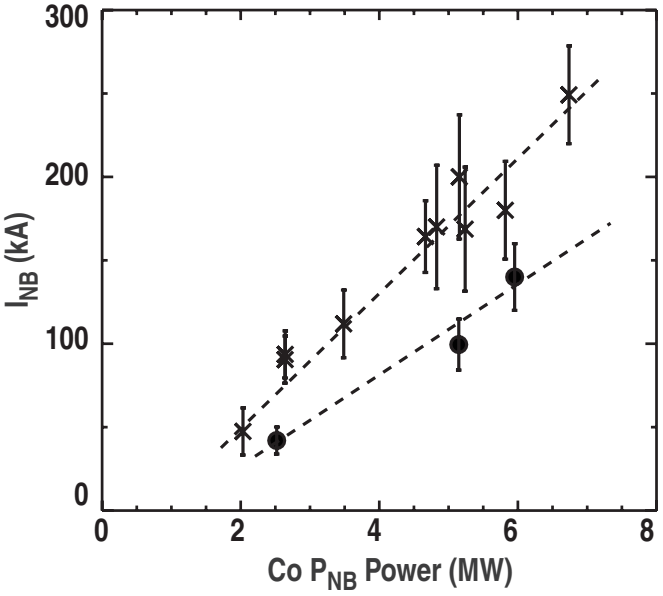

FIG. 17. Measured NBCD as a function of coinjection power for (×) favorable and (●) unfavorable alignment configurations.

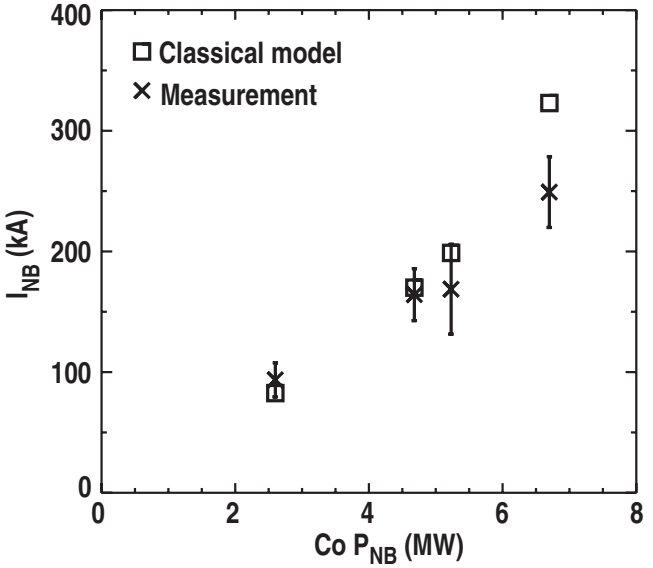

FIG. 18. Comparison of measured NBCD with NUBEAM model with $D_b=0$ for different injection powers (upshifted plasma with $+B_T$, favorable alignment configuration)

simulation with $D_b=0$ for $P_{NB}=7.2$ MW but is in good agreement for the lower power cases.[37,38] Additional information on the fast ion profile in the NB power scan is obtained from equilibrium reconstructions, since the fast ion pressure contributes to the Shafranov shift that is easily measured by the MSE polarimetry. The thermal pressure p_{th} from the n_e, T_e, T_i, and carbon density measurements is subtracted from the total plasma pressure p_{tot} from MSE equilibrium reconstruction to obtain the fast ion pressure profile p_f.[39] The measured p_f is smaller than the theoretical calculation with $D_b=0$ at the highest NB power (Fig. 20), indicating that deviation of the measured I_{NB} from the classical model for this case is correlated with fast ion loss by additional anomalous transport that increases with the injection power. As for the NBCD profile, the fast ion profile from MSE equilibrium reconstruction fits best with the theoretical calculation with $D_b=0$ and 0.3 m^2/s at $P_{NB}=5.6$ MW and 7.2 MW, respectively (Fig. 21).

Figure 22(a) shows the NBCD efficiency as a function of P_{NB}. The CD efficiency depends on the plasma parameters [Fig. 22(b)]. The measured CD efficiency increases with P_{NB}

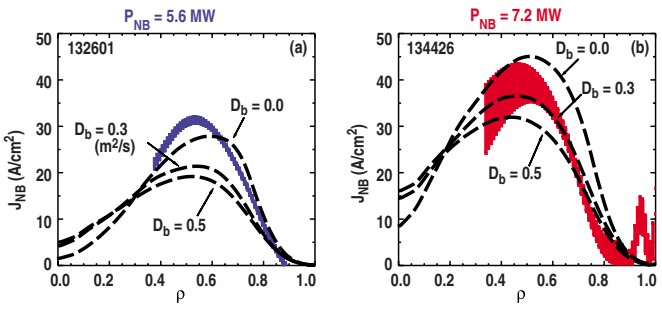

FIG. 19. (Color online) Effects of *ad hoc* anomalous fast ion diffusion on off-axis NBCD profiles. The measured NBCD profile fits best with the theoretical calculation with $D_b=0$ and 0.3 m^2/s at (a)$P_{NB}=5.6$ MW and (b) 7.2 MW, respectively.

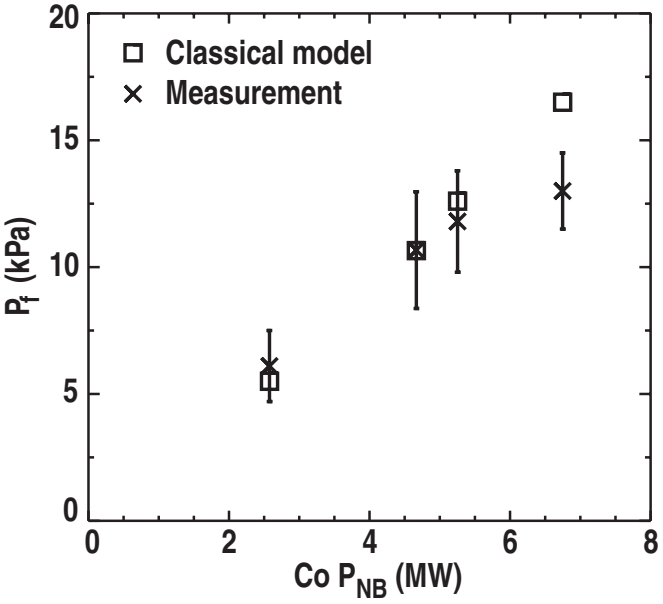

FIG. 20. Measured fast ion pressure at $\rho=0.6$ as a function of coinjection power.

primarily due to longer slowing down time for higher electron temperature. The increased Z_{eff} at higher P_{NB} reduces the electron cancellation current, resulting in additional increases in the CD efficiency. Off-axis NBCD is robust over a wide range of injection power even though a modest anomaly was observed at high NB power.

V. SUMMARY

Robust off-axis NBCD was found in DIII-D experiments using vertically shifted small plasmas. Clear evidence for off-axis NBCD was observed in the global behavior of discharges including a decrease in the internal inductance and a delay in the start time of sawteeth that results from the broader current profile compared with on-axis injection. Simulations of the MSE polarimetry signals during the current profile evolution are consistent with the measured MSE signals only when the predicted off-axis NBCD is included. The measured on- and off-axis NBCD radial profiles deduced from Ohm's law and the poloidal magnetic flux evolution constrained by the magnetic field pitch angles from the MSE polarimetry agree well with the theoretical calculations using the orbit-following Monte Carlo code. Short beam pulses show fast ions are confined as expected for on- and off-axis injections. The 2D FIDA image shows a clear off-axis beam ion profile consistent with theory.

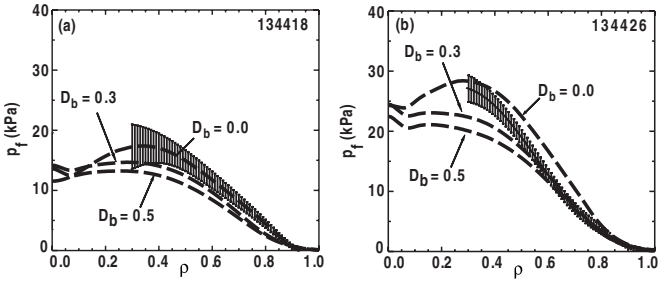

FIG. 21. Effects of *ad hoc* anomalous fast ion diffusion on beam ion pressure profiles. The measured pressure profile fits best with the theoretical calculation with $D_b=0$ and 0.3 m^2/s at (a) $P_{\text{NB}}=5.6$ MW and (b) 7.2 MW, respectively. The error bars represent random errors inferred from the variance of the time series during the stationary phase of the discharge.

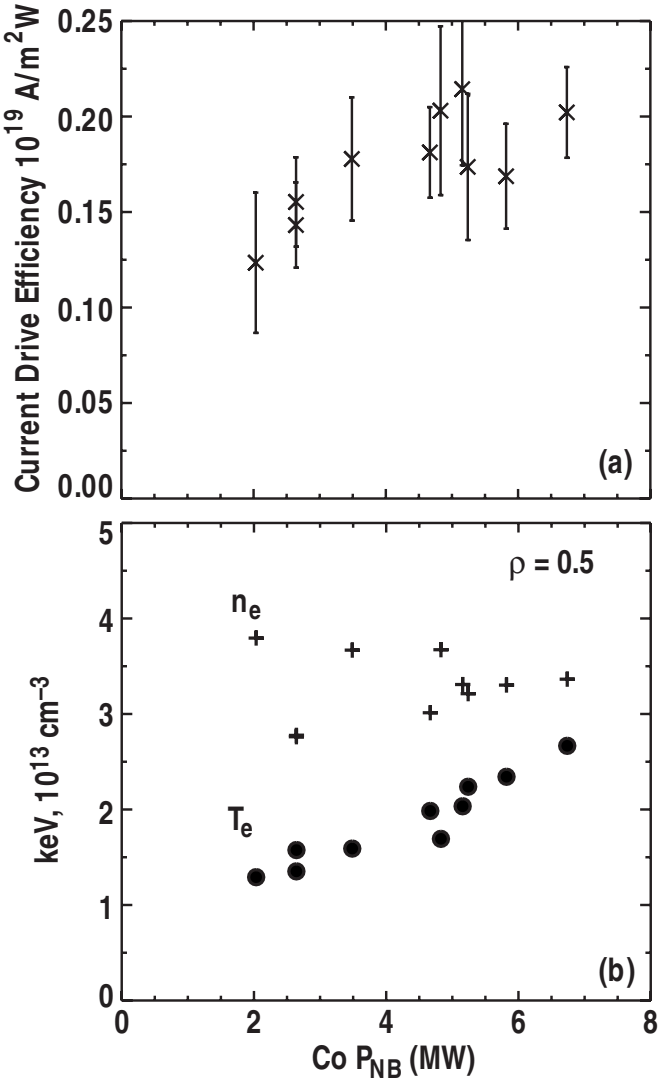

FIG. 22. (a) Measured NBCD efficiency as a function of injection power, and (b) electron density (+) and temperature (●) at $\rho=0.5$ as a function of injection power.

These experiments elucidate inherent differences between on- and off-axis NBCD. Experiments confirmed the prediction that off-axis NBCD efficiency is sensitive to the B_T direction due to alignment of the NBI with the local pitch of the magnetic field lines. If the sign of B_T yields the proper helicity, both measurement and calculation indicate that off-axis NBCD does not lose CD efficiency by being applied at a larger radius because the increased fraction of trapped electrons reduces the electron shielding of the injected ion current. The NB power scan indicates that the measured off-axis NBCD increases approximately linearly with NB power; at the highest NB power (7.2 MW), a small amount of anomalous diffusion (~ 0.3 m^2/s) needs to be introduced to bring observations and predictions into agreement. No obvious

evidence was observed that off-axis NBCD is more prone to anomalous fast ion transport than on-axis NBCD.

These experiments and modeling support the future modification of two existing DIII-D NB lines to provide off-axis NBCD as far out as half the plasma radius by vertically steering the beams downward. This system will strongly support scenario development for ITER and future tokamak reactors by allowing additional current profile control, and will provide a flexible scientific tool for understanding transport, energetic particles, heating, and CD physics.

ACKNOWLEDGMENTS

This work was supported in part by the U.S. Department of Energy under Contract Nos. DE-AC05-00OR22725, DE-FC02-04ER54698, SC-G903402, DE-FG03-97ER54415, DE-AC02-76CH03073, DE-AC52-07NA27344, DE-FG02-07ER54917, DE-FG02-89ER53297, and DE-AC05-06OR23100.

[1] W. Heidbrink and G. J. Sadler, Nucl. Fusion **34**, 535 (1994).
[2] T. S. Taylor, Plasma Phys. Controlled Fusion **39**, B47 (1997).
[3] T. C. Luce, Fusion Sci. Technol. **48**, 1212 (2005).
[4] R. J. Bickerton, J. W. Connor, and J. B. Taylor, Nature (London), Phys. Sci. **229**, 110 (1971).
[5] M. R. Wade, M. Murakami, T. C. Luce, J. R. Ferron, C. C. Petty, D. P. Brennan, A. M. Garofalo, C. M. Greenfield, A. W. Hyatt, R. Jayakumar, J. E. Kinsey, R. J. La Haye, L. L. Lao, J. Lohr, P. A. Politzer, R. Prater, E. J. Strait, and J. G. Watkins, Nucl. Fusion **43**, 634 (2003).
[6] M. Murakami, C. M. Greenfield, M. R. Wade, T. C. Luce, J. R. Ferron, H. E. St. John, M. A. Makowski, M. E. Austin, S. L. Allen, D. P. Brennan, K. H. Burrell, T. A. Casper, J. C. DeBoo, E. J. Doyle, A. M. Garofalo, P. Gohil, I. A. Gorelov, R. J. Groebner, J. Hobirk, A. W. Hyatt, R. J. Jayakumar, K. Kajiwara, C. E. Kessel, J. E. Kinsey, R. J. La Haye, J. Y. Kim, L. L. Lao, J. Lohr, J. E. Menard, C. C. Petty, T. W. Petrie, R. I. Pinsker, P. A. Politzer, R. Prater, T. L. Rhodes, A. C. C. Sips, G. M. Staebler, T. S. Taylor, G. Wang, W. P. West, L. Zeng, and DIII-D Team, Nucl. Fusion **45**, 1419 (2005).
[7] M. Murakami, M. R. Wade, C. M. Greenfield, T. C. Luce, J. R. Ferron, H. E. St. John, J. C. DeBoo, W. W. Heidbrink, Y. Luo, M. A. Makowski, T. H. Osborne, C. C. Petty, P. A. Politzer, S. L. Allen, M. E. Austin, K. H. Burrell, T. A. Casper, E. J. Doyle, A. M. Garofalo, P. Gohil, I. A. Gorelov, R. J. Groebner, A. W. Hyatt, R. J. Jayakumar, K. Kajiwara, C. E. Kessel, J. E. Kinsey, R. J. La Haye, L. L. Lao, A. W. Leonard, J. Lohr, T. W. Petrie, R. I. Pinsker, R. Prater, T. L. Rhodes, A. C. C. Sips, G. M. Staebler, T. S. Taylor, M. A. Van Zeeland, G. Wang, W. P. West, L. Zeng, and DIII-D Team, Phys. Plasmas **13**, 056106 (2006).
[8] M. Murakami, J. M. Park, C. C. Petty, W. W. Heidbrink, T. H. Osborne, R. Prater, T. C. Luce, M. R. Wade, P. M. Anderson, M. E. Austin, N. H. Brooks, R. V. Budny, C. D. Challis, J. C. DeBoo, J. S. deGrassie, J. R. Ferron, P. Gohil, J. Hobirk, C. T. Holcomb, E. M. Hollmann, R. M. Hong, A. W. Hyatt, J. Lohr, M. J. Lanctot, M. A. Makowski, D. C. McCune, P. A. Politzer, J. T. Scoville, H. E. St John, T. Suzuki, T. S. Taylor, W. P. West, E. A. Unterberg, M. A. Van Zeeland, and J. H. Yu, Nucl. Fusion **49**, 065031 (2009).
[9] J. Hobirk, T. Oikawa, T. Fujita, T. Fukuda, S. Günter, O. Gruber, A. Isayama, Y. Kamada, M. Kikuchi, M. Maraschek, Y. Miura, A. G. Peeters, G. V. Pereverze, A. Polevoi, A. C. C. Sips, A. Stäbler, J. Stober, T. Suzuki, K. Ushigusa, ASDEX Upgrade Team, and JT-60U Team, *Proceedings of the 30th EPS Conference on Controlled Fusion and Plasma Physics*, St. Petersburg, 2003 (European Physical Society, Geneva, 2003), ECA Vol. 27A, Paper No. O-4.1B.
[10] S. Günter, G. Conway, S. daGraca, H.-U. Fahrbach, C. Forest, M. Garcia Muñoz, T. Hauff, J. Hobirk, V. Igochine, F. Jenko, K. Lackner, P. Lauber, P. McCarthy, M. Maraschek, P. Martin, E. Poli, K. Sassenberg, E. Strumberger, G. Tardini, E. Wolfrom, H. Zohm, and ASDEX Upgrade Team, Nucl. Fusion **47**, 920 (2007).
[11] S. Ide, O. Naito, T. Kondoh, Y. Ikeda, K. Ushigusa, T. Fujita, M. Matsuoka, and JT-60 Team, *Proceedings of the 15th IAEA Conference*, Seville, Spain (IAEA, Vienna, 1994) Vol. 1, p. 641.
[12] T. Suzuki, S. Ide, T. Oikawa, T. Fujita, M. Ishikawa, M. Seki, G. Matsunaga, T. Hatae, O. Naito, K. Hamamatsu, M. Sueoka, H. Hosoyama, M. Nakazato, and JT-60 Team, Nucl. Fusion **48**, 045002 (2008).
[13] M. R. Tournianski, R. J. Akers, D. L. Keeling, P. G. Carolan, and G. Cunningham, *Proceedings of the 33rd EPS Conference on Plasma Physics*, Rome, 2006 (European Physical Society, Geneva, 2006), ECA Vol. 30I, Paper No. P-1.099.
[14] M. Turnyanskiy, D. L. Keeling, R. J. Akers, G. Cunningham, N. J. Conway, H. Meyer, C. A. Michael, and S. D. Pinches, Nucl. Fusion **49**, 065002 (2009).
[15] I. T. Chapman, I. Jenkins, R. V. Budny, J. P. Graves, S. D. Pinches, S. Saarelma, and JET EFDA Contributors, Plasma Phys. Controlled Fusion **50**, 045006 (2008).
[16] Y. Shimomura, M. Murakami, A. R. Polevoi, P. Barabaschi, V. Mukhovatov, and M. Shimada, Plasma Phys. Controlled Fusion **43**, A385 (2001).
[17] B. W. Rice, K. H. Burrell, L. L. Lao, and Y. R. Lin-Liu, Phys. Rev. Lett. **79**, 2694 (1997).
[18] A. Pankin, D. McCune, R. Andre, G. Bateman, and A. Kritz, Comput. Phys. Commun. **159**, 157 (2004).
[19] R. Hong, A. P. Colleraine, J. S. Haskovec, D. Kellman, J. Kim, A. Nerem, J. C. Phillips, B. Sleaford, J. J. Wight, and M. C. Vella, *Proceedings of the 12th Symposium on Fusion Engineering*, Monterey, 1987 (IEEE, Piscataway, NJ, 1988), Vol. 2, p. 1133.
[20] T. N. Carlstrom, G. L. Campbell, J. C. DeBoo, R. Evanko, and J. Evans, Rev. Sci. Instrum. **63**, 4901 (1992).
[21] Z. Wang, J. Lohr, G. L. Bell, C. Hsieh, J. Luo, R. E. Stockdale, J. B. Wilgen, and J. Zhang, *Proceedings of the 9th International Workshop on Electron Cyclotron Emission and Electron Cyclotron Heating*, Borrego Springs, 1995 (World Scientific, Singapore, 1995), p. 427.
[22] P. Gohil, K. H. Burrell, R. J. Groebner, and R. P. Seraydarian, Rev. Sci. Instrum. **61**, 2949 (1990).
[23] R. J. Hawryluk, *Physics Close to Thermonuclear Conditions* (Commission of the European Communities, Brussels, 1980), Vol. 1, p. 19.
[24] W. A. Houlberg, K. C. Shaing, S. P. Hirshman, and M. C. Zarnstorff, Phys. Plasmas **4**, 3230 (1997).
[25] C. B. Forest, K. Kupfer, T. C. Luce, P. A. Politzer, L. L. Lao, M. R. Wade, D. G. Whyte, and D. Wroblewski, Phys. Rev. Lett. **73**, 2444 (1994).
[26] L. L. Lao, J. R. Ferron, R. J. Groebner, W. Howl, H. St. John, E. J. Strait, and T. S. Taylor, Nucl. Fusion **30**, 1035 (1990).
[27] H. E. St. John, T. S. Taylor, Y. R. Lin-Liu, and A. D. Turnbull, *Proceedings of the 15th International Conference on Plasma Physics and Controlled Nuclear Fusion Research*, Seville, Spain, 1994 (IAEA, Vienna, 1995), Vol. 3, p. 603.
[28] S. P. Hirshman and D. J. Sigmar, Nucl. Fusion **21**, 1079 (1981).
[29] O. Sauter, C. Angioni, and Y. R. Lin-Liu, Phys. Plasmas **6**, 2834 (1999).
[30] C. B. Forest, C. C. Petty, F. W. Baity, S. C. Chiu, J. S. DeGrassie, K. Kupfer, R. J. Groebner, E. F. Jaeger, M. Murakami, R. I. Pinsker, R. Prater, B. W. Rice, M. R. Wade, and D. G. Whyte, Phys. Plasmas **3**, 2846 (1996).
[31] K. H. Burrell, Phys. Plasmas **4**, 1499 (1997).
[32] C. C. Petty, R. Prater, J. Lohr, T. C. Luce, W. R. Fox, R. W. Harvey, J. E. Kinsey, L. L. Lao, and M. A. Makowski, Nucl. Fusion **42**, 1366 (2002).
[33] W. W. Heidbrink, K. H. Burrell, Y. Luo, N. Pablant, and E. Ruskov, Plasma Phys. Controlled Fusion **46**, 1855 (2004).
[34] M. A. Van Zeeland, W. W. Heidbrink, and J. H. Yu, Plasma Phys. Controlled Fusion **51**, 055001 (2009).
[35] W. W. Heidbrink, M. Miah, D. Darrow, B. LeBlanc, S. S. Medley, A. L. Roquemore, and F. E. Cecil, Nucl. Fusion **43**, 883 (2003).
[36] M. Murakami, J. M. Park, T. C. Luce, M. R. Wade, and R. M. Hong, Fusion Sci. Technol. **54**, 994 (2008).
[37] W. W. Heidbrink, M. Murakami, J. M. Park, C. C. Petty, M. A. Van Zeeland, and J. H. Yu, "Beam-ion confinement for different injection geometries," Plasma Phys. Controlled Fusion (submitted).
[38] W. W. Heidbrink, J. M. Park, M. Murakami, C. C. Petty, M. A. Van Zeeland, and C. T. Holcomb, "Observation of fast-ion transport by microturbulence," Phys. Rev. Lett. (submitted).
[39] C. C. Petty, C. B. Forest, R. I. Pinsker, J. S. deGrassie, F. W. Baity, R. W. Callis, W. P. Cary, S. C. Chiu, R. L. Freeman, P. Gohil, R. J. Groebner, H. Ikezi, E. F. Jaeger, Y. R. Lin-Liu, M. Murakami, M. Porkolab, R. Prater, and B. W. Rice, *Proceedings of the 12th Topical Conference on Radio Frequency Power in Plasmas*, Savannah, 1997 (AIP, New York, 1997), p. 225.